Applied Surface Science 421 (2017) 611–616

Contents lists available at ScienceDirect

Applied Surface Science

journal homepage: www.elsevier.com/locate/apsusc

Full Length Article

Dielectric functions of La-based cuprate superconductors for visible and near-infrared wavelengths

Minglin Zhao[a], Jie Lian (Ph.D.)[a,*], Heshan Yu[b], Kui Jin[b], Liping Xu[c], Zhigao Hu[c], Xiulun Yang[a], Shishou Kang[d]

[a] School of Information Science and Engineering, Shandong University, Jinan 250100, Shandong, PR China
[b] National Lab for Superconductivity, Institute of Physics, Chinese Academy of Sciences, Beijing 100190, PR China
[c] Key Laboratory of Polar Materials and Devices, Ministry of Education, East China Normal University, Shanghai, 200241, PR China
[d] School of Physics, Shandong University, Jinan 250100, Shandong, PR China

ARTICLE INFO

Article history:
Received 27 June 2016
Received in revised form 8 October 2016
Accepted 9 October 2016
Available online 15 October 2016

Keywords:
N-type superconductor
Ellipsometry
Dielectric function
XPS

ABSTRACT

The highly c-axis oriented $La_{1.9}Ce_{0.1}CuO_4$ (LCCO) film was prepared on $SrTiO_3$ (STO) substrate by pulsed-laser deposition (PLD). The identification and characterization of the LCCO film was determined by X-ray diffraction (XRD), atomic force microscopy (AFM), scanning electron microscope (SEM) and X-ray photoelectron spectroscopy (XPS). Spectroscopic ellipsometry (SE) measurement was performed on the LCCO film in 0.5–4.13 eV range. The complex pseudodielectric function of the LCCO film was reported by Drude and Lorentz oscillators in this work. Critical point analysis on third-derivative spectra of the Lorentz contributions was accomplished to obtain the interband transition energies. The results indicate that the interband transitions are mainly related to the copper-oxygen planes. The metallic behavior of the pseudodielectric function, which is a common feature in all known electron-doped superconductors, can be obviously observed in the LCCO film.

1. Introduction

The electron-doped cuprate superconductors in the form of $R_{2-x}Ce_xCuO_4$ (R = La, Pr, Nd, Sm and Eu) [1–3], are particularly interesting because electrons, rather than holes, in the planes are suggested to be the charge carriers involved in the high T_c superconductivity [4]. The dielectric behavior has been tempting to suggest the possibility of a common origin of ferroelectricity and high T_c supeconductivity in electron-doped superconductors [5,6]. At the same time, it is also a most convenient way of characterizing the frequency-dependent optical and electronic properties of the normal state of high T_c superconducting materials. The stability of the T'-structure depends strongly on the radius of the lanthanide ions. The larger the lanthanide radii is, the more unstable the T'-structure is. This leads to a boundary for a stable T'-structure between La and Pr [7]. Thus, the T'-structure LCCO single crystal is not available as far as we know [8–10]. LCCO exhibits the highest transition temperatures (T_c = 30 K) [11], and the widest doping range for superconductivity in electron-doped cuprates [12,13]. However, there are few reports about the dielectric function of LCCO films as a result of the reasons given above. Due to an excellent lattice match between $SrTiO_3$ (STO) (a = 3.905 Å) and T'-structure (a = 4.015 Å for optimally doped LCCO), c-axis optimally-doped LCCO epitaxial thin film with great quality can be fabricated on [001]-oriented STO substrate, and we can obtain a-b plane pseudodielectric function of the LCCO by studying this epitaxial film.

In the present paper, LCCO thin film was prepared by pulsed laser deposition on STO substrate. The X-ray diffraction and X-ray photoelectron spectroscopy were performed to characterize the microstructure and the valence states involved in the interband transitions of the LCCO film, respectively. We measured pseudodielectric function spectra of the LCCO film in the visible and near-infrared region using high-precision spectroscopic ellipsometry. To enhance interband structures, we numerically calculated third derivatives of the Lorentz contribution of these spectra. From a detailed analysis of the derivative line shapes, we obtain the pseudodielectric response of the CuO_2 planes in the electron-doped compounds LCCO and discuss the corresponding normal state interband transitions.

* Corresponding author at: School of Information Science and Engineering, Shandong University, 27 Shanda Nanlu, 250100 Jinan, Shandong, PR China.
E-mail addresses: lianjie@sdu.edu.cn, opticsdu@163.com (J. Lian).

http://dx.doi.org/10.1016/j.apsusc.2016.10.055
0169-4332/

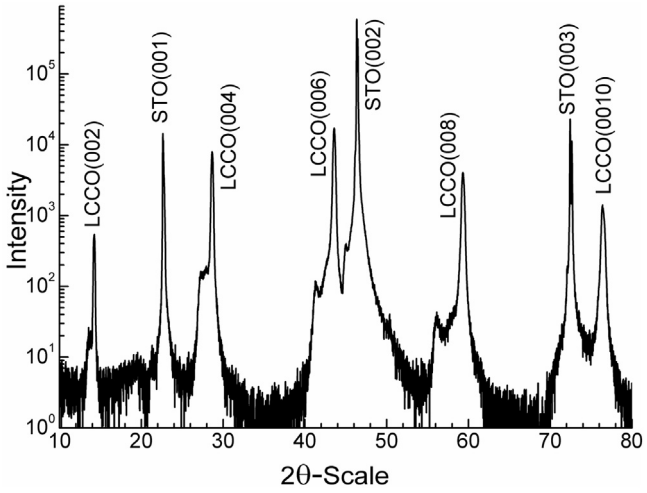

Fig. 1. X-ray Θ-2 Θ-scan of the optimal doped LCCO film at room temperature.

2. Experimental

The stoichiometric target is achieved through a conventional solid state reaction process with the atomic ratio of La:Ce:Cu:O = 1.9:0.1:1:4. The c-axis oriented film of electron-doped cuprates was deposited on the STO substrate by a pulsed laser deposition system. The grown film is about 1000 Å and controlled by the number of laser pulses. The background atmosphere before deposition is between 10^{-5} and 10^{-6} Torr, and we optimized the annealing process to achieve high transition temperature. The details of the preparation of the thin film are similar to the case of LCCO described elsewhere [13,14].

The phase and crystallinity of the LCCO thin films was characterized by X-ray diffraction (D8 Advance, Bruker AXS) with Cu-Kα = 1.54184 Å radiation. The surface morphology was characterized by atomic force microscope (NaioAFM, Nanosurf, Switzerland). The electron microscopic investigation was conducted by a 5 kV scanning electron microscope (SEM), Hitachi-S4800 FESEM, equipped with a cold field emission system and with an EDX unit (EMAX). X-ray photoelectron spectroscopy (XPS) studies were conducted with an ESCALAB 250 instrument (VG Instrument Group Ltd., UK) with a monochromatic Al-K Alpha source (1253.6 eV). The ellipsometric measurement was carried out at room temperature in the photon energy range of 0.5–4.13 eV using ultraviolet–near infrared spectroscopic ellipsometry (V-VASE by J. A. Woollam, Inc.). The measurements were performed at the angles of incidence of 75° and 70° for the LCCO thin film. In the analysis, optical modelling was performed using the software WINELLI supplied by SOPRA GES5 SE. The combination of a Drude model and a set of Lorentz oscillators are used to fit our data.

3. Results and discussion

3.1. XRD analyses of the LCCO

The XRD pattern of LCCO film for x = 0.1 is shown in Fig. 1. From the XRD data, we clearly identify the typical expected [001]-oriented T'-structure as the main phase. Additional small peaks located before the T'-structure peaks are attributed to slightly residual T-structure. The superconductivity in LCCO samples is present in T'-structure, which can be obtained by proper annealing treatments to remove the apical oxygen ions in a CuO6 octahedron of T-structure.

3.2. SEM analyses of the LCCO

The surface morphology of the LCCO film is obtained by scanning electron microscope. The high-quality and uniform surface with a small quantity of voids and particles are clearly present in Fig. 2(a). In the larger magnification SEM image Fig. 2(b), we can observe the uniformly distributed nano size grains with clear boundaries. The grains are highly elongated along the grown direction (perpendicular to the surface). This indicates that the LCCO film is single phase and has good crystallinity. The bright island observed in Fig. 2(c) is due to CuO_x (Cu_2O or CuO) particle. As reported by Kim and Gaskell [15], LCCO is unstable toward decomposition and produces Cu_2O during the annealing process.

3.3. XPS analyses of the LCCO

The La 3d state of LCCO is presented in Fig. 3. Due to the spin-orbit interaction, La 3d state splits into two peaks $3d_{3/2}$ and $3d_{5/2}$ at about 849.4 eV and 832.57 eV, respectively. Each spin-orbit split component has a complex double-peak structure typical of La^{3+} compounds [16]. The splitting energy is about 16.8 eV, which is the same of La_2O_3, and suggests that La ions are in an oxide environment in the LCCO film. Next, the XPS spectra of Ce dopant in the T'-structure LCCO is shown in Fig. 4. Because of the low Ce concentration (about 1.43 at.%), the resolution of the spectra is poor with a rather high background and rather complex to discuss. Fortunately, as suggested by Tsukada [17,18], we know that the valence of Ce is close to Ce^{4+} in T'-structure LCCO. In Fig. 5, the valence-band XPS spectra of LCCO is compared with those of $Nd_{1.85}Ce_{0.15}CuO_4$ (NCCO) [19], Cu_2O and CuO [20]. The Cu 2p spectra of LCCO contain both the features of Cu_2O and CuO. This suggests that the average valence state of Cu ion should be smaller than +2, which means a mixed valence of Cu^+ and Cu^{2+}. The Cu 2p spectra of LCCO is very similar to that of NCCO, which is the best studied electron-doped cuprate superconductor. Since the interband transitions involving electronic states in the Cu-O planes, we can suppose that the two dielectric function curves should have many similar characteristics.

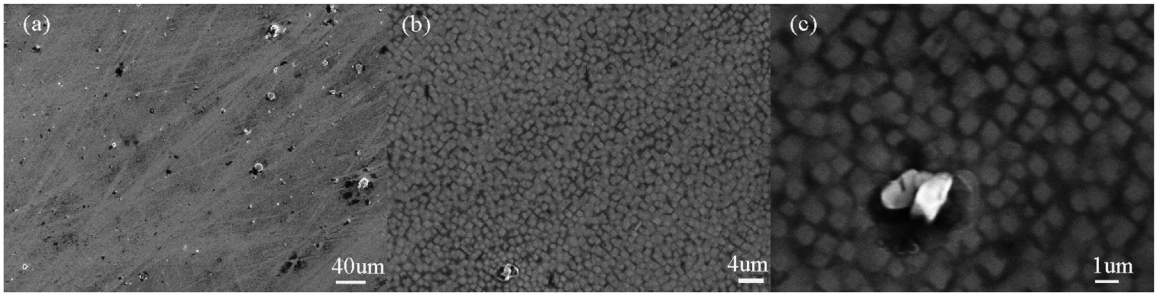

Fig. 2. Scanning electron microphotographs of the LCCO film. (a) Survey of the morphology of the LCCO film. (b) Crystalline grains of the LCCO film. (c) Impurity particles (Cu_2O or CuO) on the film surface.

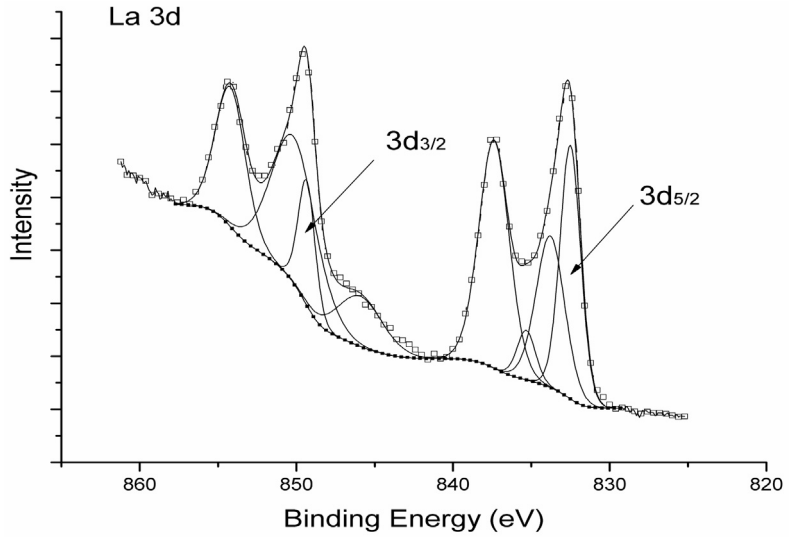

Fig. 3. La_{3d} core level XPS spectra of LCCO thin film.

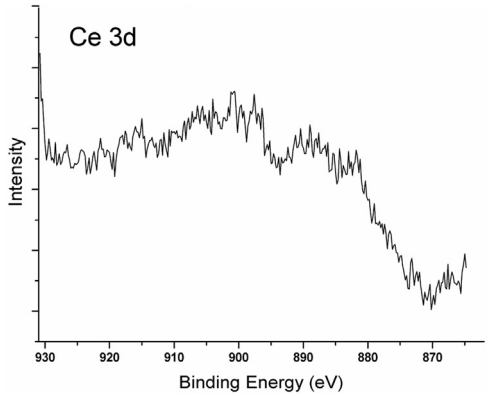

Fig. 4. Ce_{3d} core level XPS spectra of LCCO thin film.

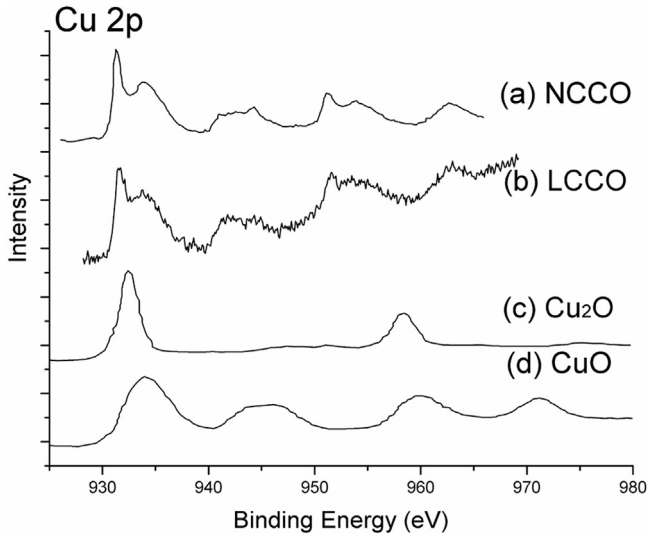

Fig. 5. Cu_{3d} core level XPS spectra of compounds. (a) NCCO data from Ref. 19, (b) LCCO, (c) Cu_2O data from Ref. [20], (d) CuO data from Ref. [20].

3.4. SE analyses of the LCCO

As a sensitive and nondestructive optical method, SE based on the reflectance configuration is easily acceptable for the determination of dielectric functions [21]. The general relationship between incident and reflected light beams is given by [22]:

$$\begin{pmatrix} E_{rp} \\ E_{rs} \end{pmatrix} = \begin{pmatrix} R_{pp} & R_{ps} \\ R_{sp} & R_{ss} \end{pmatrix} \begin{pmatrix} E_{ip} \\ E_{is} \end{pmatrix} \quad (1)$$

The nondiagonal elements of the reflection matrix lead to a mixing of s and p polarizations. These elements vanish ($R_{sp} = R_{ps} = 0$) in isotropic media and uniaxial media with its optic axis perpendicular to the surface. For the LCCO system (and all other high-T_c cuprates), the optical anisotropy exists in the dielectric tensor components representing the c-axis and a-b plane direction [23,24]. Meanwhile, for epitaxial thin films, it is rather difficult to independently obtain the c-axis component and ab-axis component by ellipsometric measurement. Fortunately, in the present case, our samples are oriented with the optical axis perpendicular to the surface. The pseudodielectric function contains all the spectral features of a-b planes and the influence of the c-axis is small [25]. The pseudodielectric function follows the equation:

$$\langle \varepsilon \rangle = \langle \varepsilon_r \rangle + i\langle \varepsilon_i \rangle = \sin^2\theta_i \left[1 + \tan^2\theta_i \left(\frac{1-\rho}{1+\rho} \right)^2 \right] \quad (2)$$

Where θ_i is the angle of incidence of light and $\rho = \tan\Psi \exp(i\Delta)$ [26].

Fig. 6 shows the experimental and simulated ellipsometric data ($\tan\Psi$and$\cos\Delta$) for LCCO at the incidence angles of 70° and 75°. In this work, the pseudodielectric function is derived from a four-layer model (air/surface roughness/LCCO film/STO substrate). The surface roughness layer was modeled by Bruggeman effective-medium approximation (EMA) with a mixture of the material (50%) and voids (50%). The best fit for the pseudodielelctric function of the LCCO film was achieved using one Drude oscillator [27] and four Lorentz oscillators [27]. The Drude-Lorentz (DL) dispersion model is given by:

$$\text{Drude}: \ \varepsilon_r = P - D^2 * \lambda^2 / \left(1 + (\lambda * E)^2\right) \quad (3)$$

$$\varepsilon_i = E * D^2 * \lambda^3 / \left(1 + (\lambda * E)^2\right) \quad (4)$$

$$\text{Lorentz}: \ \varepsilon_r = A * \lambda^2 * \left(\lambda^2 - L_0^2\right) / \left[\left(\lambda^2 - L_0^2\right)^2 + \gamma^2 * \lambda^2\right] \quad (5)$$

$$\varepsilon_i = A * \lambda^3 * \gamma / \left[\left(\lambda^2 - L_0^2\right)^2 + \gamma^2 * \lambda^2\right] \quad (6)$$

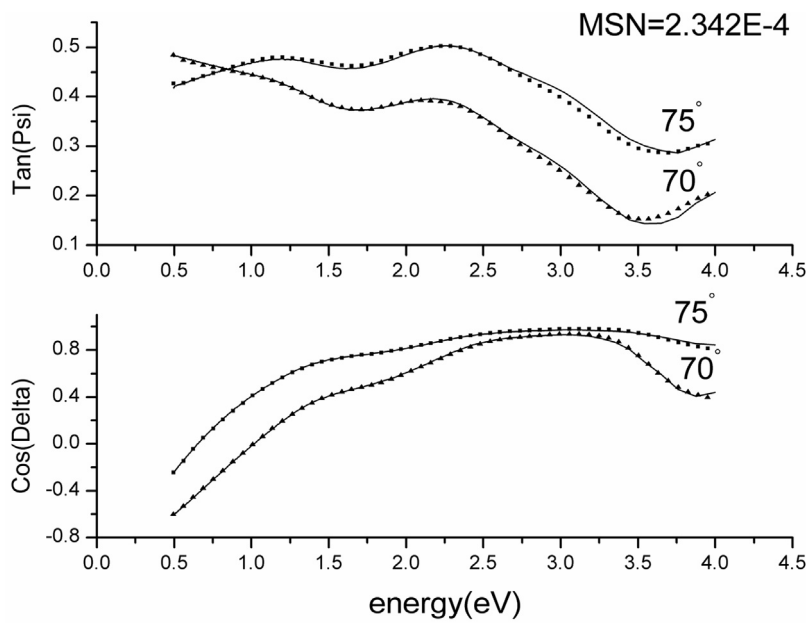

Fig. 6. Ellipsometric experimental datas (lines) and simulated datas (dots) of the $La_{2-x}Ce_xCuO4$ (x = 0.1) film at two incidence angles 70° and 75°.

Table 1
The best fitting DL parameters for the LCCO film at room temperature.

Lorentz		A	L_0(um) ↔ (eV)	γ (um)
	Peak 1	6.7212	1.3187 ↔ 0.94	2.5057
	Peak 2	0.2299	0.6672 ↔ 1.86	0.2153
	Peak 3	0.0901	0.4334 ↔ 2.86	0.1162
	Peak 4	1.4471	0.2616 ↔ 4.74	0.0814
Drude	P	D (um^{-1})	E → 1/tau (um^{-1})	
	2.8163	1.9019	0.2947	

For Drude oscillator, P is the polarization, D is the inverse of the plasma wavelength and E is the mean free path. For Lorentz oscillator, A is the intensity, L_0 the central wavelength and γ is the width of the peak. The goodness of the optical model is defined via the unbiased estimator that is the error function (MSE) [28]:

$$MSE = \frac{1}{2n-m-1} \sum_{i=1}^{n} \left[\left(\tan \psi_{cal}^{i} - \tan \psi_{\exp}^{i} \right)^2 + \left(\cos \Delta_{cal}^{i} - \cos \Delta_{\exp}^{i} \right)^2 \right] \quad (7)$$

where n is the number of measured ψ and Δ pairs included in the fit, m is the number of fit parameters and finally, cal and exp refer to theoretically calculated data and experimentally measured data respectively. The thickness of the LCCO film is 82.8 ± 2.3 nm. The thickness of the roughness layer can be fitted to about 2.658 nm from ellipsometric measurement, which agrees well with the data of the surface morphology by AFM (R_a = 2.42 nm). Based on the best fitting result, the best fitting parameters of Drude-Lorentz model are listed in Table 1. The fitting results of the pseudodielectric function $\langle \varepsilon \rangle$ are plotted with solid lines in Fig. 7, dashed lines represent only the Drude component. The pseudodielectric function of the LCCO exhibits a typical metallic behavior at energies below 2 eV, in this case, this phenomenon is clearly dominated by the free carriers caused by doping. The features at higher energy range are related to the interband transitions.

The third derivative of the pseudodielectric function with respect to photon energy enhances structures in the spectra, thus enabling more accurate lineshape analysis. To obtain the precise

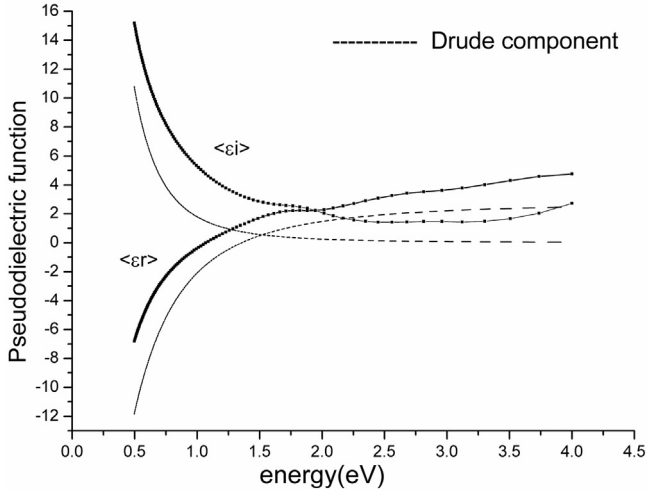

Fig. 7. Complex pseudodielectric function (dot-line) of the LCCO film. Drude component of the pseudodielectric function (dotted line).

energies of the transitions, we subtract the fitted Drude contribution and numerically calculate the third derivative of the Lorentz contribution multiplied by the square of the photon energy E. The original 100-point spectra were made an interpolation to get fixed energy steps and expanded to 250 points. The spectra was then differentiated using a three-point third derivative routine with coefficients tabulated by Savitzky and Golay [29]. This routine was found to give adequately faithful but smooth derivatives for the sample. The resulting spectra can be fitted via [30]

$$\frac{d^3}{dE^3}\left(E^2\bar{\varepsilon}\right) = \sum_{j=1}^{4} \exp\left(i\phi_j\right) \frac{C_j}{\left(E + i \cdot \Gamma_j - E_{g,j}\right)^{n/2}} \quad (8)$$

Where ϕ_j, C_j, Γ_j and $E_{g,j}$ represent the phase angle, the magnitude, the broadening energy and the transition energy of the j-th critical point, respectively. With n = 6 corresponding to a two dimensional critical point, we obtain excellent agreement with the experimental data, the parameters of the third derivative are listed in Table 2.

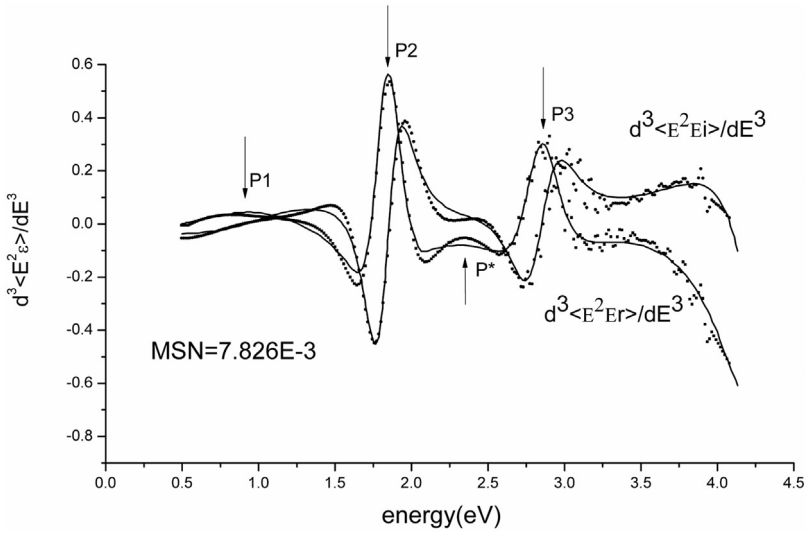

Fig. 8. Third derivative of the Lorentz contribution of pseudielectric function. Experimental (dots), Simulated(lines).

Table 2
The parameters of the third derivative of the Lorentz contribution of the pseudodielectric function.

	C	Eg (eV)	Γ (eV)	ϕ (deg)
Peak 1	0.0256	0.9475	0.7528	127.3604
Peak 2	8.2493E-3	1.8348	0.1798	114.1623
Peak 3	9.1821E-3	2.8438	0.2416	121.4684
Peak 4	0.1333	4.4672	0.4294	59.0132

The third derivative spectra reveal a three-peak structures labeled as P_i (i = 1, 2 and 3) in Fig. 8. The transition P_1 placed at around 0.95 eV is nearly vanished, and we attribute this broad peak to indirect excitations via inelastic scattering of the free carriers [31]. The transition P_2 near 1.83 eV is attributed to the charge transfer gap that occurs between the occupied Zhang-Rice singlet band (O 2p states) and the empty upper Hubbard band (Cu $3dx^2$-y^2 states), which takes place in undoped La_2CuO_4 at about 2 eV [32]. The P_3 located around 2.84 eV is observed in many copper oxide compounds such as $YBa_2Cu_3O_{7-x}$ and $SmBa_2Cu_3O_{7-x}$, and is probably related to transitions from the top of the nonbonding states (centered at 2.5 eV below E_F and ending at 0.6 eV below E_F) to the antibonding maximum with a maximum near 2 eV above E_F [33]. The weak shoulder located at about 2.35 eV is labeled as P^*, although it is not involved in the peak fitting. Similar to NCCO, this peak is ascribed to the transition between O 2p states and the upper edge of the Cu 3d states, according to Alonso's work [34]. Except for the above mentioned features, Table 1 and Table 2 show that there should still exist a peak feature located at about 4 ~ 5 eV. Due to the fact that our maximum energy limit is 4.13 eV, we can't obtain its precise value and there is a relatively large difference between the values of this peak obtained by two methods, but we could confirm its existence through the analysis of the ellipsometric spectra and the third derivative. This higher transition is ascribed to a transition from occupied O 2p states to an empty Cu state such as Cu 4s [35].

4. Conclusion

In summary, the single phase $La_{1.9}Ce_{0.1}CuO_4$ superconducting thin film was grown on STO substrate by PLD. Composition and chemical state of element are analyzed by XPS. The quality and the microstructure are determined by XRD and SEM. By applying an appropriate approach, we have determined the pseudodielectric function of LCCO film at room temperature by SE in the spectral range from 0.5-4.13 eV. Except for the Drude-like metallic response, our results give and enlighten the interband transitions located at around 0.95 eV, 1.83 eV, 2.35 eV, 2.84 eV and 4 ~ 5 eV. The results show that the behavior of electronic structure of LCCO in the normal state is similar to that of the electron doped cuprates as well as the hole doped cuprates.

Acknowledgments

This work is supported by grants from National Key Basic Research Program of China, No. 2015CB921003, fundamental research funds of Shandong University under grants No. 2016JC027.

References

[1] Y. Krockenberger, J. Kurian, A. Winkler, A. Tsukada, M. Naito, L. Alff, Superconductivity phase diagrams for the electron-doped cuprates $R_{2-x}Ce_xCuO_4$ (R = La, Pr, Nd, Sm, and Eu), Phys. Rev. B 77 (6) (2008) 060505.
[2] N.P. Armitage, P. Fournier, R.L. Greene, Progress and perspectives on electron-doped cuprates, Rev. Mod. Phys. 82 (3) (2010) 2421.
[3] B. Chesca, M. Selfrled, T. Dahm, N. Schopohl, D. Koelle, R. Klelner, A. Tsukada, Observation of Andreev bound states in bicrystal grain-boundary Josephson junctions of the electron-doped superconductor $La_{2-x}Ce_xCuO_{4-y}$, Phys. Rev. B 71 (10) (2005) 104504.
[4] H. Takagi, S. Uchida, Y. Tokura, Superconductivity produced by electron doping in CuO 2-layered compounds, Phys. Rev. Lett. 62 (10) (1989) 1197.
[5] C.C. Homes, B.P. Clayman, Optical properties of $Nd_{1.85}Ce_{0.15}CuO_4$, Phys. Rev. B 56 (9) (1997) 5525–5534.
[6] A. Zimmers, J.M. Tomczak, R.P.S.M. Lobo, N. Bontemps, C.P. Hill, M.C. Barr, Y. Dagan, R.L. Greene, A.J. Millis, C.C. Homes, Infrared properties of electron-doped cuprates: tracking normal-state gaps and quantum critical behavior in $Pr_{2-x}Ce_xCuO_4$, Europhys. Lett. 70 (2) (2005) 225–231.
[7] M. Naito, H. Markus, Superconducting T′-$La_{2-x}Ce_xCuO_4$ films grown by molecular beam epitaxy, Jpn. J. Appl. Phys. 39 (2000) 485–487.
[8] K. Oka, H. Shibata, S. Kashiwaya, H. Eisaki, Crystal growth of $La_{2-x}Ce_xCuO_4$, Physica C 388 (2003) 389–390.
[9] M. Fujita, M. Nakagawa, C.D. Frost, K. Yamada, High-energy spin excitations in heavily electron-doped $Pr_{1-x}LaCe_xCuO_4$, J. Phys: Conf. Ser. 108 (2008) 012006.
[10] A.N. Lavrov, H.J. Kang, Y. Kurita, T. Suzuki, S. Komiya, J.W. Lynn, S.H. Lee, P. Dai, Y. Ando, Spin-flop transition and the anisotropic magnetoresistance of $Pr_{1.3-x}La_{0.7}Ce_xCuO_4$: unexpectedly strong spin-charge coupling in the electron-doped cuprates, Phys. Rev. Lett. 92 (2004) 227003.
[11] K. Jin, X.H. Zhang, P. Bach, R.L. Greene, Evidence for antiferromagnetic order in $La_{2-x}Ce_xCuO_4$ from angular magnetoresistance measurements, Phys. Rev. B 80 (2009) 012501.
[12] B.X. Wu, K. Jin, J. Yuan, H.B. Wang, T. Hatano, B.R. Zhao, B.Y. Zhu, Preparation of electron-doped $La_{2-x}Ce_xCuO_{4\pm\delta}$ thin films with various Ce doping by dc magnetron sputtering, Physic C 469 (2009) 1945–1949.
[13] H. Wu, L. Zhao, J. Yuan, L.X. Cao, J.P. Zhong, L.J. Gao, B. Xu, P.C. Dai, B.Y. Zhu, B.R. Zhao, Transport properties of electron-doped $La_{2-x}Ce_xCuO_4$ cuprate thin films, Phys. Rev. B 73 (2006) 104512.

[14] K. Jin, J. Yuan, L. Zhao, H. Wu, X.Y. Qi, B.Y. Zhu, L.X. Cao, X.G. Qiu, B. Xu, X.F. Duan, B.R. Zhao, Coexistence of superconductivity and ferromagnetism in a dilute cobalt-doped $La_{1.89}Ce_{0.11}CuO_{4\pm\delta}$ system, Phys. Rev. B 74 (2006) 094518.
[15] J.S. Kim, D.R. Gaskell, The phase stability diagrams for the systems $Nd_2CuO_{4-\delta}$ and $Nd_{1.85}$ $Ce_{0.15}CuO_{4-\delta}$, Physica C 209 (1993) 381–388.
[16] B. Viswanathan, S. Madhavan, C.S. Swamy, Charge transfer satellites in X-ray photoelectron spectra of La_2CuO_4, Phys. Status. Solidi. B 133 (2) (1986) 629–632.
[17] A. Tsukada, M. Naito, H. Yamamoto, Valence of ce in T-and T′-$La_{2-x}Ce_xCuO_4$, Physica C 463 (2007) 64–67.
[18] A. Tsukada, H. Yamamoto, M. Naito, Doping of Ce in T-La_2CuO_4: rigorous test for electron-hole symmetry for high-T c superconductivity, Phys. Rev. B 74 (17) (2006) 174515.
[19] M. Taguchi, A. Chainani, K. Horiba, et al., Evidence for suppressed screening on the surface of high temperature $La_{2-x}Sr_xCuO_4$ and $Nd_{2-x}Ce_xCuO_4$ superconductors, Phys. Rev. Lett. 95 (17) (2005) 177002.
[20] D. Tahir, S. Tougaard, Electronic and optical properties of Cu, CuO and Cu_2O studied by electron spectroscopy, J. Phys-Condens. Mat. 24 (17) (2012) 175002.
[21] H. Zhigao, W. Genshui, H. Zhiming, M. Xiangjian, S. Fuwen, C. Junhao, Investigations of the optical properties of $Ba_{0.9}Sr_{0.1}TiO_3$ ferroelectric thin films by spectroscopic ellipsometry, Jpn. J. Appl. Phys. 42 (3R) (2005) 1400.
[22] R.M.A. Azzam, N.M. Bashara, Ellipsometry and Polarized Light North-Holland, New York, 1977.
[23] A. Pimenov, A.V. Pronin, A. Loidl, A. Tsukada, M. Naito, Peak in the far-infrared conductivity of strongly anisotropic cuprates, Phys. Rev. B 66 (2002) 212508.
[24] D. van der Marel, Anisotropy of the optical conductivity of high-Tc cuprates, Phys. Rev. B 60 (1999) 765–768.
[25] M.I. Alonso, S. Tortosa, M. Garriga, S. Piñol, Ellipsometric measurement of the dielectric tensor of $Nd_{2-x}Ce_xCuO_{4-\delta}$, Phys. Rev. B 55 (5) (1997) 3216–3221.
[26] D.E. Aspnes, A.A. Studna, Dielectric functions and optical parameters of si, ge, gap, gaas, gasb, inp, inas, and insb from 1.5 to 6.0 ev, Phys. Rev. B 27 (2) (1983) 985.
[27] Handbook of Ellipsometry, in: H.G. Tompkins, E.A. Irene (Eds.), William Andrew, New York, 2005.
[28] O. Messaoudi, H. Makhlouf, A. Souissi, I. Benassaker, M. Karyaoui, A. Bardaoui, M. Oueslati, R. Chtourou, Correlation between optical and structural properties of copper oxide electrodeposited on ITO glass, J. Alloy Compd. 611 (2014) 142–148.
[29] A. Savitzky, M.J.E. Golay, Smoothing and differentiation of data by simplified least squares procedures, Anal. Chem. 36 (8) (1964) 1627–1639.
[30] D.E. Aspnes, Third-derivative modulation spectroscopy with low-field electroreflectance, Surf. Sci. 37 (1973) 418–442.
[31] H.P. Geserich, G. Scheiber, J. Geerk, H.C. Li, G. Linker, W. Assmus, W. Weber, Optical spectra of superconducting $YBa_2Cu_3O_{7-\delta}$ films: evidence for Cu^{++} d-d transitions, Europhys. Lett. 6 (3) (1988) 277–282.
[32] A.S. Moskvin, True charge-transfer gap in parent insulating cuprates, Phys. Rev. B 84 (7) (2011) 075116.
[33] M. Garriga, J. Humlíček, J. Barth, R.L. Johnson, M. Cardona, Ellipsometric measurements of high-T_c compounds, J. Opt. Soc. Am. B 6 (1989) 470–474.
[34] M.I. Alonso, M. Garriga, S. Piñol, M. Brinkmann, Doping dependence of the ellipsometric spectra of $Nd_{2-x}Ce_xCuO_{4-\delta}$ single crystals, Physica C 299 (1998) 41–51.
[35] J. Bäckström, D. Budelmann, R. Rauer, M. Rübhausen, Optical properties of $YBa_2Cu_3O_{7-\delta}$ and $PrBa_2Cu_3O_{7-\delta}$ films: high-energy correlations and metallicity, Phys. Rev. B 70 (17) (2004) 174502.